THE JOURNAL OF PHYSICAL CHEMISTRY C
A JOURNAL OF THE AMERICAN CHEMICAL SOCIETY

pubs.acs.org/JPCC

Article

Cavity-Enhanced Raman Scattering from 2D Hybrid Perovskites

Aditya Singh, Jason Lynch, Surendra B. Anantharaman, Jin Hou, Simrjit Singh, Gwangwoo Kim, Aditya D. Mohite, Rajendra Singh, and Deep Jariwala*

Cite This: *J. Phys. Chem. C* 2022, 126, 11158−11164

Read Online

ACCESS | Metrics & More | Article Recommendations | Supporting Information

ABSTRACT: Two-dimensional (2D) hybrid organic−inorganic perovskites (HOIPs) are promising candidates for optoelectronic applications due to their efficient light emission properties and strong dielectric confinement effects. Raman spectroscopy is a versatile, non-contact, and often non-destructive technique, widely used to characterize crystalline materials. However, the weak phonon scattering, strong background, and complex nature of the Raman signals from HOIPs present challenges in obtaining reliable signals. Furthermore, the fragile nature of the 2D HOIP crystals results in rapid degradation upon exposure to heat, light, and moisture, which presents further difficulty in enhancing Raman scattered photon signals. Herein, we report a novel approach to enhance the weak Raman scattering signals in Ruddlesden-Popper phase HOIPs by introducing an open-cavity comprising the HOIP crystals on a gold substrate. We observe 15x enhancement of the Raman signals due to the Purcell effect inside the high-index HOIP crystals. Our simple approach can be extended to enhance the study of phonon scattering in other HOIPs and van der Waals layered crystals.

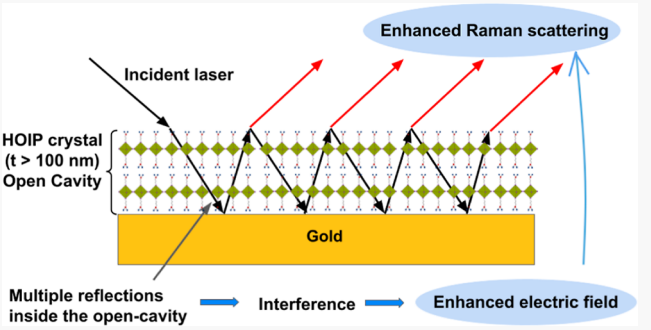

1. INTRODUCTION

Two-dimensional (2D) Ruddlesden-Popper (RP) hybrid organic−inorganic perovskites (HOIPs) have attracted much attention due to their uniquely tunable structure, strong quantum confinement, and extraordinary performance in optoelectronic devices.[1] The RP phase of these HOIPs have a layered crystal structure represented by the chemical formula $(RNH_3)_2(MNH_3)_{n-1}A_nX_{3n+1}$, where "R" is an alkyl or aromatic moiety, "M" is a methyl group ($-CH_3$), "A" is a metal cation (Pb), "X" is a halide (I, Cl, Br), and "*n*" is an integer that defines the number of inorganic (PbI_2) layers of corner-sharing $[PbI_6]^{4-}$ octahedra confined by two adjacent organic layers.[2] $[PbI_6]^{4-}$ layers act as quantum wells, and organic layers act as dielectric spacers, which play a crucial role in charge confinement, hydrophobicity, structural rigidity, and stability.[3]

Physical properties of HOIPs such as charge confinement can be tuned by the integer *n*, electron−phonon (e-p) coupling by the organic moiety, and band structure by halide anions and external strain.[3,4] Furthermore, the e-p coupling is responsible for scattering and provides decay channels for the excitons, which leads to the determination of absorption and emission properties of the material.[5,6] Also, due to the tender and ionic lattice of HOIPs, which is readily deformable under laser exposure, e-p coupling induces polaronic nature in excitons, leading to intricate excited-state phenomena.[7] In lead halide 2D perovskites, polaronic character exhibits a crucial role in carrier transport and excitation dynamics, leading to long carrier lifetime, slow thermalization of hot carriers, and weak dephasing rates.[8] Therefore, investigation of vibrational dynamics of HOIPs is of paramount importance as they possess the information about e-p interaction, structural and compositional changes, symmetry of lattice vibration, temperature and pressure phase diagram, degree of crystallinity, dielectric screening, and elastic properties of the crystal.[2,3]

Raman spectroscopy plays a crucial role in the study of vibrational dynamics of materials. Unfortunately, HOIPs have weak optical phonon scattering and strong background from the relaxation of electronic excited states[9] when excited above the band gap. In addition, several overlapping and complex Raman modes smother crucial information about their vibrational spectra and properties.[10] HOIPs exposed to excessive power of laser excitation within the band gap of the material are prone to degradation due to the thermal stress induced by the laser.[10−12] Degradation in HOIP crystals introduces additional Raman peak artifacts, making the characterization of the material and the assignment of the modes very complex and challenging.[3,13,14] These material challenges/limitations compel the search and development of a consistent technique or means to characterize the vibrational

Received: March 5, 2022
Revised: June 16, 2022
Published: July 1, 2022

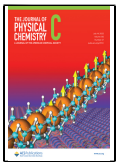

https://doi.org/10.1021/acs.jpcc.2c01577
J. Phys. Chem. C 2022, 126, 11158−11164

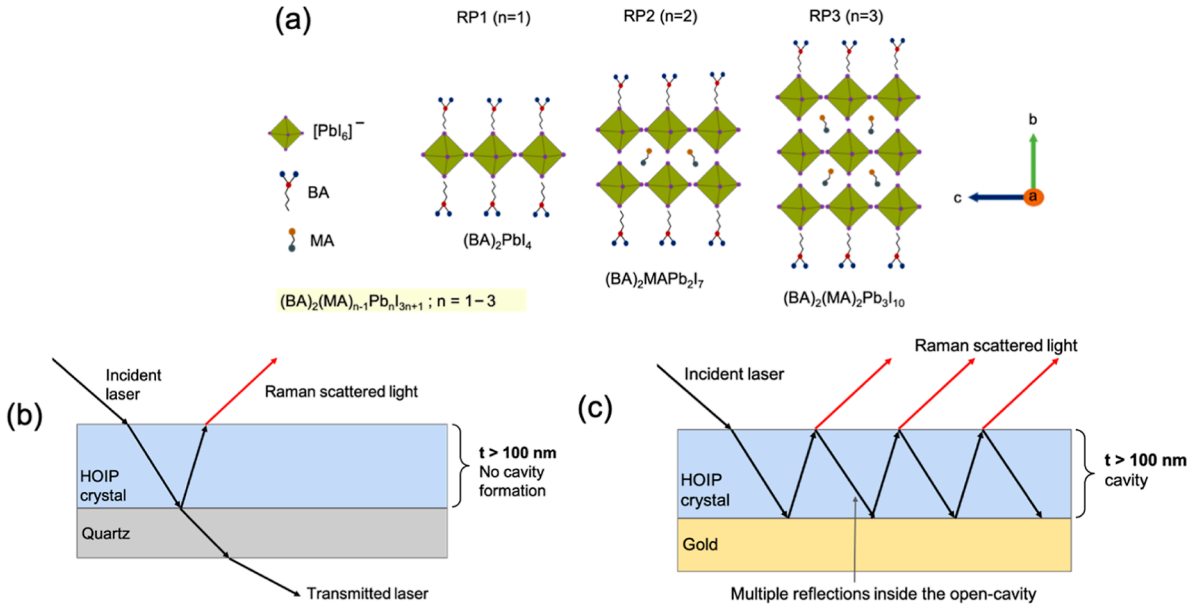

Figure 1. Schematic illustration of enhanced Raman signals from 2D RP HOIPs due to cavity formation. (a) Schematic of the crystal structure of RP phase 2D hybrid butylamine (BA) lead iodide-based perovskites, where n is the number of inorganic layers of $[PbI_6]^{4-}$between two organic layers. (b) Schematic of the interaction of the incident laser with thick (t > 100 nm) HOIP crystals placed over a quartz substrate. Lasers (photons) interact with crystals, scattering occurs, and lasers transmit through the quartz substrate. (c) When the quartz substrate is replaced by optically thick gold, the reflected laser beam interferes with the incoming beam. The black arrow shows the electric field propagation direction of the pump laser, whereas the red arrow shows the electric field propagation direction of the scattered. Note: the incident laser shown in this schematic is at an angle, while in Raman experiments/electric field simulation, the laser is at normal incidence over the crystal surface.

spectra from such environment-sensitive materials via Raman scattering.

HOIPs have a crystal lattice that intrinsically exhibits low probability for Raman scattering. Enhancement in Raman scattering can be achieved by electromagnetic enhancement by placing the semiconductor over metallic nanoparticles for surface-enhanced Raman spectroscopy or placing them between nanogap metallic cavities for tip-enhanced Raman spectroscopy.[15] However, the aforementioned material limitations in terms of thermal and chemical stability constitute a significant drawback in enhancing the phonon scattering from the HOIP crystals.

In this paper, we fabricate an open-cavity comprising the RP perovskite flakes on a gold substrate (which acts as a reflector) and exploit the Purcell effect to increase the probability of Raman scattering by enhancing light trapping in the crystal. The extraordinary optical constants of HOIP crystals facilitate the strong light-matter coupling in thick crystals (thickness, t > 100 nm), which leads to photonic open-cavity formation in crystals themselves.[1,16] When the laser shines on the HOIP/gold, the laser undergoes multiple reflections inside the dielectric cavity created by the flat surfaces of the HOIP crystal. Due to the Purcell effect inside the crystals, the optical electric field is enhanced, which results in enhanced Raman scattering by a factor of up to 15x. Our work exhibits a simple approach to enhance the Raman scattering, which can be extended to enhance phonon scattering in other van der Waals crystals.

2. EXPERIMENTAL METHODS

Sample Preparation. Gold template substrates were prepared by depositing a 100 nm thick film of gold on a silicon wafer, and a mixer of two epoxy components was dropped over it. Silicon substrates were placed over epoxy drops and heated to 100 °C for 30 min. After cooling, template-stripped gold substrates were ready to use.[17] HOIPs in RP phase flakes were exfoliated from the single-crystal samples by the scotch-tape method inside the glovebox to avoid moisture and sample degradation.

Optical Characterization. Raman scattering and reflectance measurements were performed by 600 grooves/mm grating and 50x objective (NA = 0.35) in the Horiba LabRam HR Evolution system under the vacuum (10^{-5} torr) using the Linkam stage. For low-temperature measurements, liquid nitrogen was used as a coolant in the Linkam stage. Raman scattering measurements were carried out using 633 and 785 nm laser wavelengths as the excitation source. To avoid the laser heating-induced effect in the RP crystals, we had optimized the experimental conditions such as laser power and integration time to observe detectable Raman signals with high signal-to-noise ratios. We found that thick RP/gold crystals can sustain high laser power without perovskite disintegration up to ∼1 mW for the 785 nm laser and up to ∼500 μW for the 633 nm laser at 80 K. Reflectance measurements of samples were recorded by illuminating the external white light source on the samples. Reflectance from the silver mirror was used to normalize the reflectance data and to avoid the effect of gold substrate absorption in the reflectance data of samples.

Atomic Force Microscopy. Thickness and surface topography of samples were measured by OmegaScope Smart SPM (AIST).

Electric Field Distribution Simulations. The transfer-matrix method (TMM) was implemented using python based on the theory presented in the ref 18 to simulate the electric field (E-field) distribution profiles of 633 and 785 nm lasers for RPn placed on quartz and gold substrates. Required optical

https://doi.org/10.1021/acs.jpcc.2c01577
J. Phys. Chem. C 2022, 126, 11158−11164

constants of RPn have been obtained from ellipsometry measurements.[16]

3. RESULTS AND DISCUSSION

Figure 1a shows the schematic of the crystal structure of RP phase lead iodide-based HOIPs whose general chemical formula is $(BA)_2(MA)_{n-1}Pb_nI_{3n+1}$, where BA is butylammonium and MA is methylammonium.[2,3] Therefore, RPn (n = 1, 2, 3...) can be chemically expressed as $(BA)_2PbI_4$, $(BA)_2(MA)Pb_2I_7$, and $(BA)_2(MA)_2Pb_3I_{10}$ or in short, RP1, RP2, and RP3, respectively. In our previous work,[1] we reported that thick (t > 100 nm) RP HOIP crystals placed on gold show strong light-matter coupling (exciton−polariton formation) and form an open-cavity with a quality factor ∼250. Here, we exploit the Purcell effect in HOIPs to enhance the emission of Raman scattering, using the 633 and 785 nm lasers, which are far from the excitonic absorption (Figure S1, Supporting Information). Purcell proposed that the spontaneous emission rate can be modified (enhanced) by placing the emitter inside a cavity.[19] Using the Purcell effect, enhanced radiative emission from a variety of semiconducting and atomic systems has been reported.[20,21] Here, we use the same phenomenon for enhancing the Raman scattering signals from a weak phonon scattering crystal such as 2D HOIPs.

In our samples, light is trapped inside the cavity due to multireflection from the bottom gold substrate and top HOIP crystal−air interface. The required minimum volume of the cavity under the diffraction limit is approximately calculated by

$$0.1\left(\frac{\lambda_0}{n'}\right)^3 \quad (1)$$

where λ_0 is the free-space wavelength of light and n' is the refractive index of the material inside the cavity.[22] Refractive indices of RP1, RP2, and RP3 for λ_0 = 785 (633) nm wavelength was obtained from spectroscopic ellipsometry as 2.1 (2.2), 2.2 (2.4), and 2.3 (2.7), respectively.[16] Therefore, from eq 1, it turns out that all three RPn achieve the minimum size/thickness of the cavity to trap light in crystals that are $\gtrsim$ 100 nm at wavelengths of 633 and 785 nm, which are primary pump lasers for the Raman scattering experiment. These theoretical calculations match well with our experimental results of reflectance, which show exciton−polariton formation in thick HOIP crystals (t > 100 nm) rather than thin ones (t < 30 nm) (Figure S1), as reported before [1].

Figure 1b depicts the interaction of the incident laser beam with the HOIP crystal placed on a quartz substrate. Due to the low reflectivity of the HOIP−quartz interface, most of the photons pass through it and do not reflect, limiting the number of reflections inside the cavity, due to which multiple reflections of the laser inside the crystal do not occur. Laser (incident photons) interacts with HOIP crystals and back-scattered signal photons collected by the objective are passed through the spectrometer to the detector. However, when the transmissive quartz substrate is replaced with a highly reflective gold substrate, the incident laser beam reflects back at the HOIP−gold interface (Figure 1c). Due to the cavity nature of 2D HOIP thick crystals (high refractive index), laser again reflects back from the top of the HOIP−air interface, which leads to multiple reflections inside the crystals. The incident and reflected laser beams undergo interference, resulting in electric field enhancement in the crystal.

Figure 2a,b shows the Raman spectra of thick HOIP/quartz and HOIP/gold measured at 80 K using a 785 nm laser source.

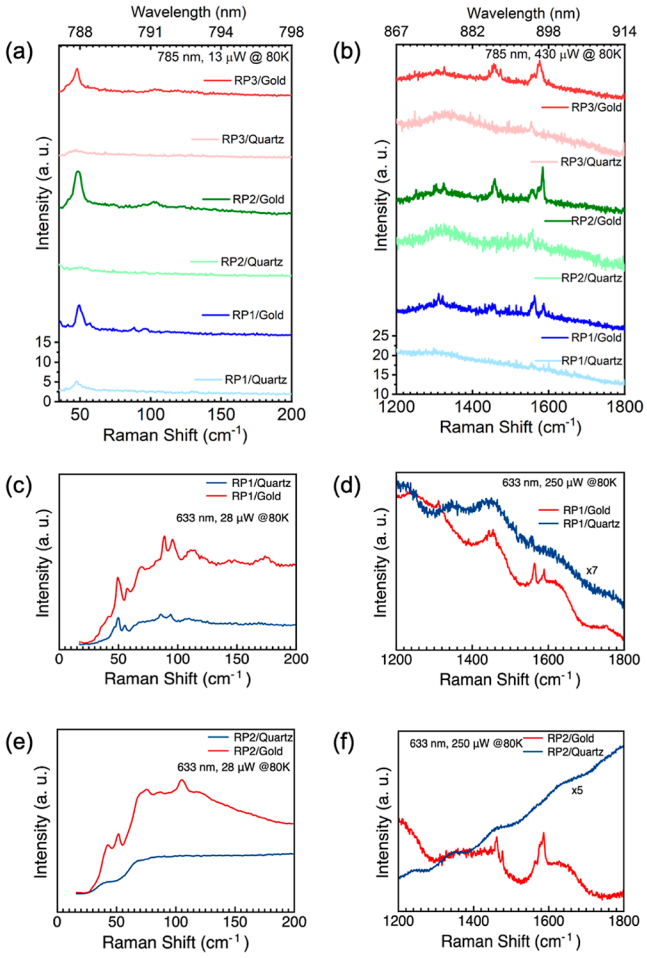

Figure 2. Cavity-enhanced Raman signals from thick crystals of RPn/gold compared to RPn/quartz measured by the 785 nm laser line (non-resonant to all RPn) at 80 K for (a) inorganic and organic layers and (b) organic layers of HOIP crystals. Raman spectra of RP1 (c,d) and RP2 (e,f) by the 633 nm laser at 80 K.

Information about Raman modes of inorganic−organic perovskites and organic spacer layers is enclosed in the range <200 cm^{-1} (range R1, hereafter) and 1200−1800 cm^{-1} (range R2, hereafter).[23] Details of frequency and character of these vibrational modes are explained in the text later. The thicknesses of these crystals have been measured by atomic force microscopy (AFM), and corresponding topographical images and height profiles are shown in Supporting Information (Figure S2). A 785 nm laser is used for pumping, which is non-resonant with the exciton−polariton modes from all three RPn used in this study (Figure S1). Therefore, the enhanced Raman intensity is purely attributed to the cavity effect rather than resonant Raman scattering. As a result, thick crystals of RPn/gold show enhanced Raman intensity up to 15x compared to RPn/quartz due to cavity-enhanced Raman scattering (see Figure 2a,b). In range R1, the Raman mode (measured by the 785 nm laser) of RPs at ≈ 48 cm^{-1}, which belongs to the PbI_3 network, has enhancement in the intensity of 3x, 15x, and 7x for RP1, RP2, and RP3, respectively (Figure 2a). However, modes at ≈92 and ≈103 cm^{-1}, and all modes of range R2 (for 785 and 633 both lasers), are very weak and

https://doi.org/10.1021/acs.jpcc.2c01577
J. Phys. Chem. C 2022, 126, 11158−11164

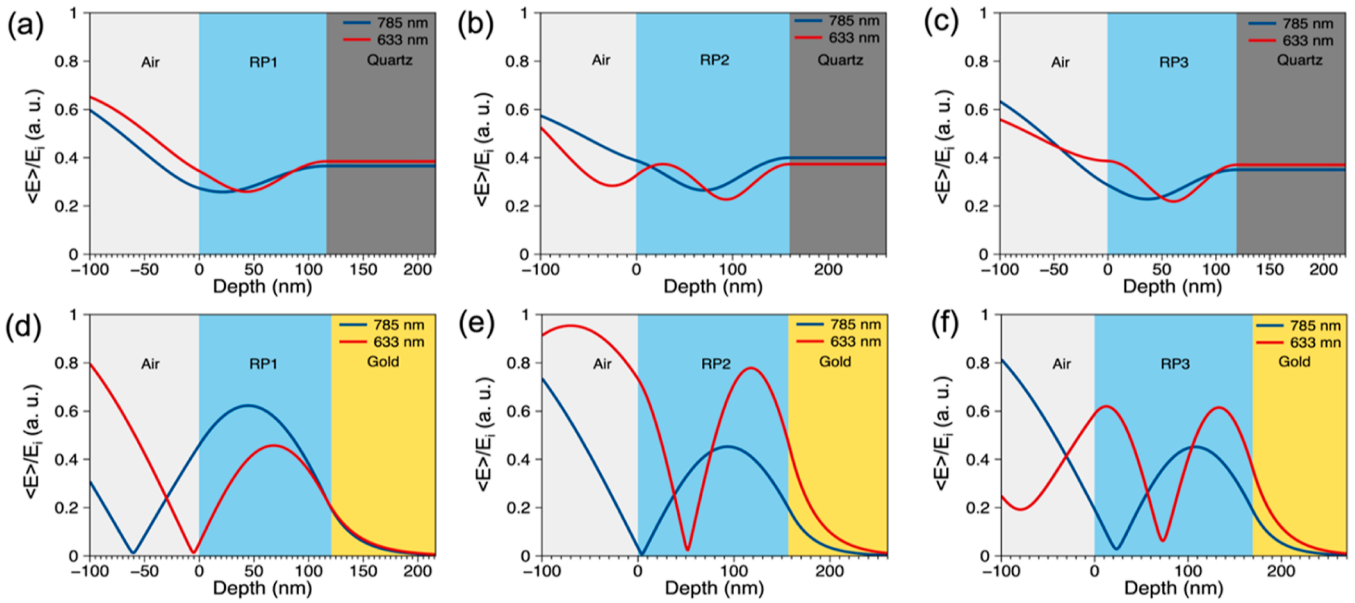

Figure 3. TMM simulations of the time-averaged electric field distribution of 633 and 785 nm lasers in thick (t > 100 nm) HOIP crystals: E-field distribution profiles (normalized to the incident E-field E_i) in thick crystals of RPn on (a−c) quartz and (d−f) gold substrate. The thickness of RP1, RP2, and RP3 crystals on quartz (gold) is 117 (120), 160 (157), and 120 (170) nm, respectively.

poorly resolved in RPs/quartz compared to RPs/gold, which restricts the quantification of enhancement in Raman intensity. Furthermore, in the case of Raman of RP1 and RP2 by the 633 nm laser, there is an enhancement of 2−3x for various modes in range R1 (Figure 2c,e).

To validate the universality of the open-cavity effect, Raman spectra of the same samples were recorded using a 633 nm excitation laser as well (Figure 2c−f). It is worth mentioning that the huge background in Raman spectra by the 633 nm laser, unlike the flat background by 785 nm, is due to our broad cutoff wavelength in the 633 nm edge filter of the Raman system (see Figure S3, Supporting Information). At 80 K, Raman signals of thick RP3 by the 633 nm laser were subjugated by polaritonic emission at ∼645 nm (see Figure S1, Supporting Information). Compared to the 785 nm laser, Raman measurements by the 633 nm laser show more well-resolved modes at low powers (<30 μW) due to the fact that (a) Raman scattering intensity is inversely proportional to the excitation wavelength and (b) sensitivity of the charge-coupled device detector decreases in the near-infrared region, which applies for the 785 nm laser wavelength.[24] Furthermore, we did Raman measurements of RP3/quartz by the 633 nm laser source and found that although it leads to near-resonant Raman scattering, the cavity effect is stronger (Figure S5).

Figure 3 shows the time-averaged E-field distribution profile of 633 and 785 nm lasers in thick crystals (t > 100 nm) of RPn/quartz and RPn/gold. The AFM measured thicknesses of RP1, RP2, and RP3 crystals on quartz (gold) are 117 (120), 160 (157), and 120 (170) nanometers, respectively (Figure S2). RPn/quartz have minimum E-field intensity near the middle of the thickness of the crystal (Figure 3a−c). Furthermore, the transparent nature of quartz makes the laser beam pass through it, leading to limited back reflection and E-field enhancement inside the crystal. However, thick HOIP crystals on gold have a maximum enhanced E-field in the crystal (Figure 3d−f). Higher optical E-fields within the crystal vis-à-vis the air-crystal and crystal−substrate interface increase the probability for the interaction between the laser beam and the phonons of HOIP crystals, which ultimately leads to enhanced Raman intensity.[22,25] We have also verified that surface plasmons do not play any significant role in this Raman intensity enhancement via a separate control experiment (see Supporting Information, S6). Using the transfer matrix method, the enhancement in the Purcell factor (F_p) was calculated by determining the Q factors and mode volumes (V_m) for the HOIPs on the SiO_2 and Au substrates (see Table 1). The change in the Purcell factor was then calculated using

Table 1. Transfer-Matrix Simulation Data for Calculating Purcell Enhancement Factors of Different HOIPs

RPn	wavelength (nm)	$\frac{Q_{Au}}{Q_{SiO2}}$	$\frac{V_m^{Au}}{V_m^{SiO2}}$	$\frac{F_p^{Au}}{F_p^{SiO2}}$
RP1	633	6.36	0.417	15.3
RP1	785	6.36	0.465	13.7
RP2	633	5.52	0.4	13.8
RP2	785	5.52	0.43	12.9
RP3	633	4.9	0.505	9.7
RP3	785	4.9	0.413	11.9

$F_p \propto \frac{Q}{V_m}$, and it was found that using the Au substrate can enhance the Purcell factor by ≈15x. This suggests that the Raman signal should also increase by a factor of 15, as observed in previous studies.[26−28]

Lattice vibrations of HOIP crystals in the Raman scattering spectra can be characterized notably into two sections: range R1 (<200 cm^{-1}), which comprise the vibrational dynamics of the inorganic layer of PbI_3 network and organic layer both, representing low wavenumbers, and range R2 (1200−1800 cm^{-1}), which contains the lattice vibration of the organic layer only.[23] Recently, Menahem et al.[29] carried out Raman spectroscopy and density functional perturbation theory of 2D $(BA)_2PbI_4$ crystals for the range <200 cm^{-1} and compared their structural dynamics with its 3D counterpart, $MAPbI_3$. They concluded that like $MAPbI_3$, $(BA)_2PbI_4$ also exhibits

https://doi.org/10.1021/acs.jpcc.2c01577
J. Phys. Chem. C 2022, 126, 11158−11164

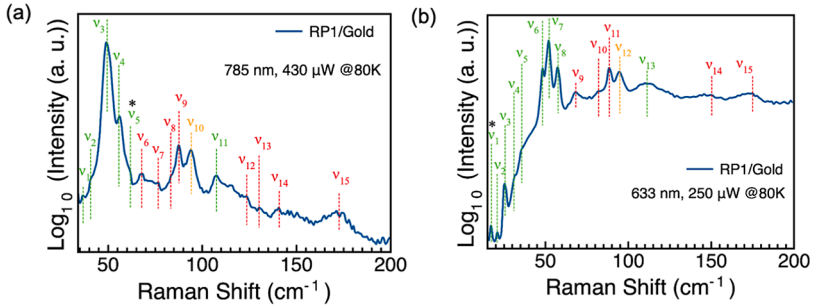

Figure 4. Application of enhanced Raman intensity: the logarithmic plot of the Raman spectra of RP1/gold at 80 K obtained via pumping (a) 785 and (b) 633 nm lasers. Raman modes in green and red belong to inorganic and organic components of the HOIPs, respectively, while modes in orange are common to both. Modes marked with asterisk (*) are theoretically predicted to be silent but have been observed in our experiments.

temperature-dependent phase transition. At room temperature, $(BA)_2PbI_4$ has a tetragonal crystal structure, while at low temperatures, it has an orthorhombic phase. Furthermore, both materials have similar vibrational dynamics, and their Raman modes appear approximately at the same positions at 80 K.[23,29] It is noteworthy that as organic spacers, BA and MA have similar chemical nature. Therefore, we can assume that the Raman features of $(BA)_2PbI_4$, are similar to that of $MAPbI_3$.

A normal mode of vibration is whether Raman- or IR-active, it depends upon its symmetry.[30] Group theory analysis shows that the symmetries of the normal vibrational modes of $MAPbI_3$ can be expressed as: $\Gamma_{optic} = 17A_u + 21B_{1u} + 16B_{2u} + 21B_{3u} + 19A_g + 14B_{1g} + 19B_{2g} + 14B_{3g}$. In the case of the inorganic PbI_3 network, A_u modes are expected to be silent, u modes are IR-active, and g modes are Raman-active.[31] Figure 4a, b shows the logarithmic plot of the Raman spectra of RP1/gold at 80 K by 785 and 633 nm lasers, respectively. We observe a wide variety of Raman peaks in the R1 range from our cavity-enhanced Raman spectra. Experimentally observed all Raman modes of RP1/gold crystal along with their symmetry assignment are tabulated in S8 and S9 (Supporting Information). Raman peaks (ν_1–ν_{15}) measured by the 785 nm laser are observed at 36.4, 40.5, 48.8, 56.2, 61.8, 67.7, 76.0, 83.4, 87.5, 94.0, 107.3, 123.4, 130.0, 146.5, and 171.3 cm^{-1} and by the 633 nm laser are observed at 17.0, 21.2, 25.3, 31.2, 35.2, 48.5, 52.1, 57.0, 67.5, 81.7, 88.5, 94.5, 111.0, 150.0, and 174.7 cm^{-1}. Raman modes <65 cm^{-1} are dominated by the PbI_3 network only, which consist of rocking and bending vibrations of Pb–I–Pb, while in the range 65–200 cm^{-1}, vibrations are either in vibration/translation modes of the organic cations or internal vibrations of the PbI_3 network.[23] As shown in Figure 4a,b, Raman modes in green and red belong to inorganic and organic layers, respectively, while the mode in orange overlaps with both. Modes marked with an asterisk (*) are theoretically silent (A_u modes) and are observed in our experiments.[23,29] Furthermore, in our enhanced Raman signals, we also observe the silent A_u modes at 17.0 and 61.8 cm^{-1} in $(BA)_2PbI_4$, which have not been reported in the literature precedent to the best of our knowledge. These theoretically silent peaks have been assigned to the Pb–I–Pb bend and Pb–I stretch modes in $MAPbI_3$, respectively.[23]

Fundamental Raman modes of the BA cation fall in the R2 range (1200–1800 cm^{-1}), which comprises the angular distortion of CH_2, CH_3, and NH_2 groups.[32,33] The observed Raman modes in our experiments in the R2 range at ≈1251 cm^{-1} correspond to CH_2 twisting, ≈1300 cm^{-1} to CH_2 wagging, ≈1458 cm^{-1} to a mixture of CH_2 scissoring vibration and CH_3 antisymmetric deformation, ≈1556 cm^{-1} to asymmetric NH_3 deformation, and ≈1584 cm^{-1} to NH_3^+ degenerate deformation, while the mode at ≈1323 cm^{-1} marked with a blue asterisk is not reported in the literature (Figure S7).[23,29,32,33] A plausible explanation for the 1323 cm^{-1} mode could be that a strong interaction between BA and MA molecules of RP2 on gold with incoming photons has led to the splitting of mode at ≈ 1320 cm^{-1} into 1300 and 1323 $cm.^{-1}$[34] This further emphasizes that the enhanced light–matter interaction leads to an increase in the intensity of the nominally weak Raman modes of HOIP crystals in addition to the observation of hitherto unknown and unseen modes.

4. CONCLUSIONS

In summary, we show that the Raman scattering in 2D HOIP crystals can be enhanced without compromising the crystal quality or need for complex integration with resonant optical elements. The E-field in the crystals and consequently phonon scattering, is enhanced via an open-cavity comprising 2D HOIP crystals of varying thicknesses on gold substrates. Due to the Purcell effect, we also observe an increase in the Raman signal intensity by a factor up to 15x including observation of new Raman modes at low wavenumbers. TMM simulations corroborate the E-field enhancement hypothesis that we deduce from experiments. Our observations provide a path forward to leverage simple cavity effects induced by a high-index sample on a reflective metal substrate to enhance the light–matter interactions and Raman scattering in materials with phonon scattering cross-sections and can be potentially also be translated to other van der Waals crystals.

■ ASSOCIATED CONTENT

Supporting Information

The Supporting Information is available free of charge at https://pubs.acs.org/doi/10.1021/acs.jpcc.2c01577.

Reflectance of thick and thin RP/gold; AFM topography and height profiles of RP (n = 1–3) crystals; Raman spectra of RP2/gold-NPs; experimentally observed Raman modes with their symmetry assignment and corresponding references; and Raman spectra of thin RP crystals (PDF)

■ AUTHOR INFORMATION

Corresponding Author

Deep Jariwala − *Department of Electrical and Systems Engineering, University of Pennsylvania, Philadelphia, Pennsylvania 19104, United States;* orcid.org/0000-0002-3570-8768; Email: dmj@seas.upenn.edu

https://doi.org/10.1021/acs.jpcc.2c01577
J. Phys. Chem. C 2022, 126, 11158–11164

Authors

Aditya Singh − *Department of Physics, Indian Institute of Technology Delhi, New Delhi 110016, India; Department of Electrical and Systems Engineering, University of Pennsylvania, Philadelphia, Pennsylvania 19104, United States*

Jason Lynch − *Department of Electrical and Systems Engineering, University of Pennsylvania, Philadelphia, Pennsylvania 19104, United States*

Surendra B. Anantharaman − *Department of Electrical and Systems Engineering, University of Pennsylvania, Philadelphia, Pennsylvania 19104, United States;* orcid.org/0000-0002-1882-5540

Jin Hou − *Department of Chemical and Biomolecular Engineering and Department of Materials Science and Nanoengineering, Rice University, Houston, Texas 77005, United States;* orcid.org/0000-0002-8786-3276

Simrjit Singh − *Department of Electrical and Systems Engineering, University of Pennsylvania, Philadelphia, Pennsylvania 19104, United States*

Gwangwoo Kim − *Department of Electrical and Systems Engineering, University of Pennsylvania, Philadelphia, Pennsylvania 19104, United States;* orcid.org/0000-0001-8519-4411

Aditya D. Mohite − *Department of Chemical and Biomolecular Engineering and Department of Materials Science and Nanoengineering, Rice University, Houston, Texas 77005, United States;* orcid.org/0000-0001-8865-409X

Rajendra Singh − *Department of Physics, Indian Institute of Technology Delhi, New Delhi 110016, India;* orcid.org/0000-0002-6890-6904

Complete contact information is available at: https://pubs.acs.org/10.1021/acs.jpcc.2c01577

Notes

The authors declare no competing financial interest.

■ ACKNOWLEDGMENTS

D.J. acknowledges primary support for this work by the U.S. Army Research Office under contract number W911NF-19-1−0109. D.J. and G.K. acknowledge partial support from the Asian office of Aerospace Research and Development (AOARD)/Air Force Office of Scientific Research (AFOSR) (grant FA2386-20-1−4074) and partial support from the National Science Foundation funded University of Pennsylvania Materials Research Science and Engineering Center (MRSEC) (DMR-1720530). D.J. and J.L. also acknowledge partial support from FA2386-21-1−4063. A.S. and S.S. acknowledge funding support from the Fulbright-Nehru Fellowship program supported by the United States-India Educational Foundation. S.B.A. gratefully acknowledges partial funding received from the Swiss National Science Foundation (SNSF) under the Early Postdoc Mobility program (grant P2ELP2_187977) to conduct this work. R.S. acknowledges partial financial support from the Nanoscale Research Facility at the Indian Institute of Technology Delhi, India.

■ REFERENCES

(1) Anantharaman, S. B.; Stevens, C. E.; Lynch, J.; Song, B.; Hou, J.; Zhang, H.; Jo, K.; Kumar, P.; Blancon, J.-C.; Mohite, A. D.; et al. Self-Hybridized Polaritonic Emission from Layered Perovskites. *Nano Lett.* **2021**, *21*, 6245−6252.

(2) Blancon, J.-C.; Even, J.; Stoumpos, C. C.; Kanatzidis, M. G.; Mohite, A. D. Semiconductor Physics of Organic−Inorganic 2D Halide Perovskites. *Nat. Nanotechnol.* **2020**, *15*, 969−985.

(3) Leng, K.; Fu, W.; Liu, Y.; Chhowalla, M.; Loh, K. P. From Bulk to Molecularly Thin Hybrid Perovskites. *Nat. Rev. Mater.* **2020**, *5*, 482−500.

(4) Zhang, L.; Geng, W.; Tong, C.-j.; Chen, X.; Cao, T.; Chen, M. Strain Induced Electronic Structure Variation in Methyl-Ammonium Lead Iodide Perovskite. *Sci. Rep.* **2018**, *8*, 7760.

(5) Gong, X.; Voznyy, O.; Jain, A.; Liu, W.; Sabatini, R.; Piontkowski, Z.; Walters, G.; Bappi, G.; Nokhrin, S.; Bushuyev, O.; et al. Electron−Phonon Interaction in Efficient Perovskite Blue Emitters. *Nat. Mater.* **2018**, *17*, 550−556.

(6) Thouin, F.; Valverde-Chávez, D. A.; Quarti, C.; Cortecchia, D.; Bargigia, I.; Beljonne, D.; Petrozza, A.; Silva, C.; Srimath Kandada, A. R. Phonon Coherences Reveal the Polaronic Character of Excitons in Two-Dimensional Lead Halide Perovskites. *Nat. Mater.* **2019**, *18*, 349−356.

(7) Tao, W.; Zhang, C.; Zhou, Q.; Zhao, Y.; Zhu, H. Momentarily Trapped Exciton Polaron in Two-Dimensional Lead Halide Perovskites. *Nat. Commun.* **2021**, *12*, 1400.

(8) Srimath Kandada, A. R.; Silva, C. Exciton Polarons in Two-Dimensional Hybrid Metal-Halide Perovskites. *J. Phys. Chem. Lett.* **2020**, *11*, 3173−3184.

(9) Quan, L. N.; Park, Y.; Guo, P.; Gao, M.; Jin, J.; Huang, J.; Copper, J. K.; Schwartzberg, A.; Schaller, R.; Limmer, D. T.; et al. Vibrational Relaxation Dynamics in Layered Perovskite Quantum Wells. *Proc. Natl. Acad. Sci. U. S. A.* **2021**, *118*, No. e2104425118.

(10) Pistor, P.; Ruiz, A.; Cabot, A.; Izquierdo-Roca, V. Advanced Raman Spectroscopy of Methylammonium Lead Iodide: Development of a Non-Destructive Characterisation Methodology. *Sci. Rep.* **2016**, *6*, 35973.

(11) Deretzis, I.; Alberti, A.; Pellegrino, G.; Smecca, E.; Giannazzo, F.; Sakai, N.; Miyasaka, T.; La Magna, A. Atomistic Origins of CH3NH3PbI3 Degradation to PbI2 in Vacuum. *Appl. Phys. Lett.* **2015**, *106*, 131904.

(12) Zhou, Y.; Garces, H. F.; Padture, N. P. Challenges in the Ambient Raman Spectroscopy Characterization of Methylammonium Lead Triiodide Perovskite Thin Films. *Front. Optoelectron.* **2016**, *9*, 81−86.

(13) Stoumpos, C. C.; Cao, D. H.; Clark, D. J.; Young, J.; Rondinelli, J. M.; Jang, J. I.; Hupp, J. T.; Kanatzidis, M. G. Ruddlesden−Popper Hybrid Lead Iodide Perovskite 2D Homologous Semiconductors. *Chem. Mater.* **2016**, *28*, 2852−2867.

(14) Stoumpos, C. C.; Soe, C. M. M.; Tsai, H.; Nie, W.; Blancon, J.-C.; Cao, D. H.; Liu, F.; Traoré, B.; Katan, C.; Even, J.; et al. High Members of the 2D Ruddlesden-Popper Halide Perovskites: Synthesis, Optical Properties, and Solar Cells of (CH3(CH2)3NH3)2-(CH3NH3)4Pb5I16. *Chem* **2017**, *2*, 427−440.

(15) Langer, J.; Jimenez de Aberasturi, D.; Aizpurua, J.; Alvarez-Puebla, R. A.; Auguié, B.; Baumberg, J. J.; Bazan, G. C.; Bell, S. E. J.; Boisen, A.; Brolo, A. G.; et al. Present and Future of Surface-Enhanced Raman Scattering. *ACS Nano* **2020**, *14*, 28−117.

(16) Song, B.; Hou, J.; Wang, H.; Sidhik, S.; Miao, J.; Gu, H.; Zhang, H.; Liu, S.; Fakhraai, Z.; Even, J.; et al. Determination of Dielectric Functions and Exciton Oscillator Strength of Two-Dimensional Hybrid Perovskites. *ACS Mater. Lett.* **2021**, *3*, 148−159.

(17) Zhang, H.; Abhiraman, B.; Zhang, Q.; Miao, J.; Jo, K.; Roccasecca, S.; Knight, M. W.; Davoyan, A. R.; Jariwala, D. Hybrid Exciton-Plasmon-Polaritons in van Der Waals Semiconductor Gratings. *Nat. Commun.* **2020**, *11*, 3552.

(18) Pettersson, L. A. A.; Roman, L. S.; Inganäs, O. Modeling Photocurrent Action Spectra of Photovoltaic Devices Based on Organic Thin Films. *J. Appl. Phys.* **1999**, *86*, 487−496.

(19) Purcell, E. M. Spontaneous Emission Probabilities at Radio Frequencies. In *Confined Electrons and Photons: New Physics and Applications*; Burstein, E., Weisbuch, C., Eds.; *NATO ASI Series*; Springer US: Boston, MA, 1995, pp 839.

(20) Adamo, G.; Swaha Krishnamoorthy, H. N.; Cortecchia, D.; Chaudhary, B.; Nalla, V.; Zheludev, N. I.; Soci, C. Metamaterial Enhancement of Metal-Halide Perovskite Luminescence. *Nano Lett.* **2020**, *20*, 7906−7911.
(21) Liang, T.; Liu, W.; Liu, X.; Li, Y.; Fan, J. Fabry−Perot Mode-Limited High-Purcell-Enhanced Spontaneous Emission from In Situ Laser-Induced CsPbBr3 Quantum Dots in CsPb2Br5 Microcavities. *Nano Lett.* **2022**, *22*, 355−365.
(22) Pelton, M. Modified Spontaneous Emission in Nanophotonic Structures. *Nat. Photonics* **2015**, *9*, 427−435.
(23) Pérez-Osorio, M. A.; Lin, Q.; Phillips, R. T.; Milot, R. L.; Herz, L. M.; Johnston, M. B.; Giustino, F. Raman Spectrum of the Organic−Inorganic Halide Perovskite CH3NH3PbI3 from First Principles and High-Resolution Low-Temperature Raman Measurements. *J. Phys. Chem. C* **2018**, *122*, 21703−21717.
(24) Larkin, P. J. *Infrared and Raman Spectroscopy: Principles and Spectral Interpretations*; Elsevier: Amsterdam, Netherlands, 2018.
(25) Jung, N.; Crowther, A. C.; Kim, N.; Kim, P.; Brus, L. Raman Enhancement on Graphene: Adsorbed and Intercalated Molecular Species. *ACS Nano* **2010**, *4*, 7005−7013.
(26) Petrak, B.; Djeu, N.; Muller, A. Purcell-Enhanced Raman Scattering from Atmospheric Gases in a High-Finesse Microcavity. *Phys. Rev. A* **2014**, *89*, 023811.
(27) Checoury, X.; Han, Z.; El Kurdi, M.; Boucaud, P. Deterministic Measurement of the Purcell Factor in Microcavities through Raman Emission. *Phys. Rev. A* **2010**, *81*, 033832.
(28) Gomez Velez, J.; Muller, A. Purcell-Enhanced Microcavity Raman Scattering from Pressurized Gases. *Appl. Phys. Lett.* **2018**, *112*, 041107.
(29) Menahem, M.; Dai, Z.; Aharon, S.; Sharma, R.; Asher, M.; Diskin-Posner, Y.; Korobko, R.; Rappe, A. M.; Yaffe, O. Strongly Anharmonic Octahedral Tilting in Two-Dimensional Hybrid Halide Perovskites. *ACS Nano* **2021**, *15*, 10153−10162.
(30) Yu, P. Y.; Cardona, M. Vibrational Properties of Semiconductors, and Electron-Phonon Interactions. In *Fundamentals of Semiconductors: Physics and Materials Properties*; Yu, P. Y., Cardona, M., Eds.; *Graduate Texts in Physics*; Springer: Berlin, Heidelberg, 2010, pp 107−158. DOI: 10.1007/978-3-642-00710-1_3
(31) Champagne, A. *Vibrational Properties of Hybrid Halide Perovskite for Solar Cells Applications*; Master Dissertation, Ecole polytechnique de Louvain, Université catholique de Louvain, 2016.
(32) Teixeira-Dias, J. J. C.; de Carvalho, L. A. E. B.; da Costa, A. M. A.; Lampreia, I. M. S.; Barbosa, E. F. G. Conformational Studies by Raman Spectroscopy and Statistical Analysis of Gauche Interactions in N-Butylamine. *Spectrochim. Acta, Part A* **1986**, *42*, 589−597.
(33) Costa, A. M. A. d.; Carvalho, L. A. E. B. d.; Teixeira-Dias, J. J. C.; Barbosa, E. F. G.; Lampreia, I. M. S. The Temperature Dependence of the Raman Spectrum and Gauche Interactions of Tri-N-Butylamine: A Conformational Study. *Can. J. Chem.* **1987**, *65*, 384−390.
(34) Dhanabalan, B.; Leng, Y.-C.; Biffi, G.; Lin, M.-L.; Tan, P.-H.; Infante, I.; Manna, L.; Arciniegas, M. P.; Krahne, R. Directional Anisotropy of the Vibrational Modes in 2D-Layered Perovskites. *ACS Nano* **2020**, *14*, 4689−4697.

https://doi.org/10.1021/acs.jpcc.2c01577
J. Phys. Chem. C 2022, 126, 11158−11164